SLAMS AT PARALLEL SHOCKS AND HOT FLOW ANOMALIES

E. A. Lucek

Imperial College, London

Email: e.lucek@imperial.ac.uk

ABSTRACT

We present a review of Cluster observations of two bow shock phenomena, using data from a range of tetrahedron scales. The first are SLAMS: magnetic field enhancements embedded within the quasi-parallel shock transition. They are thought to play an essential role in plasma thermalisation at shocks. We show that their overall size exceeds 1000 km, but that they have internal structure on scales of ~150 km, and that they evolve on time scales of a few seconds. The second phenomena are Hot Flow Anomalies (HFAs): regions of explosively expanding hot plasma generated by the interaction of a tangential discontinuity with the bow shock. We explore the shape and evolution of HFAs. Small spacecraft separation scales are particularly suited for examining the boundary motion and orientation of these structures, and we demonstrate the occurrence of shocks at the edges of the expanding HFA bubble, and compare their orientations with the estimated orientation of the underlying discontinuity. Observations at large scales are appropriate for the examination of the time evolution of the HFA structure: we show an example upstream of the bow shock in the flank region when the four spacecraft observed the evolution of shocks from compressions at the HFA edges.

1. INTRODUCTION

In this paper we present the properties of two phenomena associated with the terrestrial bow shock. We first describe the characteristics of magnetic field enhancements generated within the shock when the upstream magnetic field is nearly aligned with the normal to the nominal shock surface. These enhancements have been termed SLAMS (Short, Large-Amplitude Magnetic Structures) [1] or pulsations [2]. We then discuss the contribution Cluster observations have made to understanding the shape, size and evolution of explosive, non-linear events which can be generated at the bow shock through interaction with a tangential discontinuity in the solar wind. These events have been called Hot Flow Anomalies, but are also known as Hot Diamagnetic Cavities and Active Current Sheets [e,g. 3,4,5].
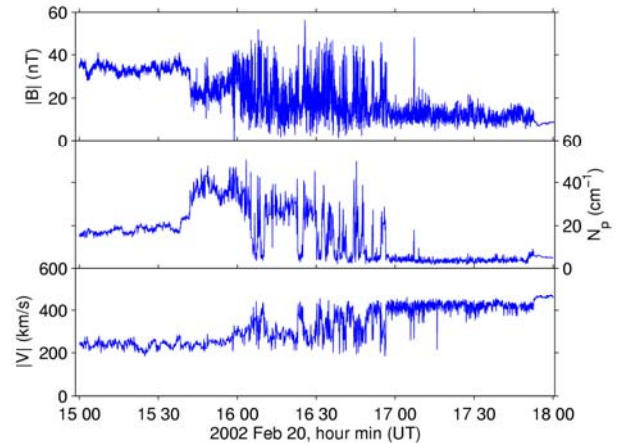

Figure 1. An example of a quasi-parallel bow shock crossing. Panels show magnetic field magnitude, |B| in nT, ion number density, N_P, in particles per cm^3 and velocity magnitude, |V|, in km/s.

The properties of the bow shock which forms ahead of the Earth depend on the upstream solar wind conditions: the solar wind velocity, which determines the strength of the shock, the plasma beta and the magnetic field direction. When the magnetic field lies close to the shock plane, and thus perpendicular to the shock normal, then the majority of ions reflected from the shock gyrate upstream, re-encounter the shock ramp, and then pass downstream [6]. In these circumstances a spacecraft crossing the shock will typically observe a short, sharp crossing. This type of shock is called a quasi-perpendicular shock. In the case where the magnetic field is more closely aligned with the normal to the nominal shock surface: a quasi-parallel shock, ions can then escape upstream where they generate ultra-low frequency (ULF) waves [7]. In such a case, unless the shock is very weak, the transition becomes extended in space, and variable in time [8]. Figure 1 shows an example of a quasi-parallel shock crossing measured by Cluster. Panels show the measured magnetic field magnitude (|B|) from the FGM instrument [9], and then ion number density (N_p) and plasma velocity magnitude (|V|) from the CIS instrument [10].

Cluster was initially located downstream of the shock. From just after 15:30 the spacecraft then encountered multiple magnetic field, density and velocity perturbations, eventually reaching undisturbed upstream flow. Dual spacecraft analysis using data from AMPTE and ISEE showed that this type of shock transition could not be explained by the simple in-out motion of a shock surface, but that the transition was instead populated by magnetic field enhancements (SLAMS) convected anti-sunward past the spacecraft [1,2]. The SLAMS were associated with decelerated and partially thermalised plasma.

Observations [11] and simulations [12] showed that the SLAMS grew as a result of the interaction between the upstream ULF waves and the gradient in energetic ion pressure upstream of the shock. In the early 1990s Schwartz and Burgess [13] developed a concept of the structure of the shock, based on dual spacecraft observations together with simulation results. A schematic of the shock transition is shown in Figure 2 [courtesy of S. J. Schwartz].
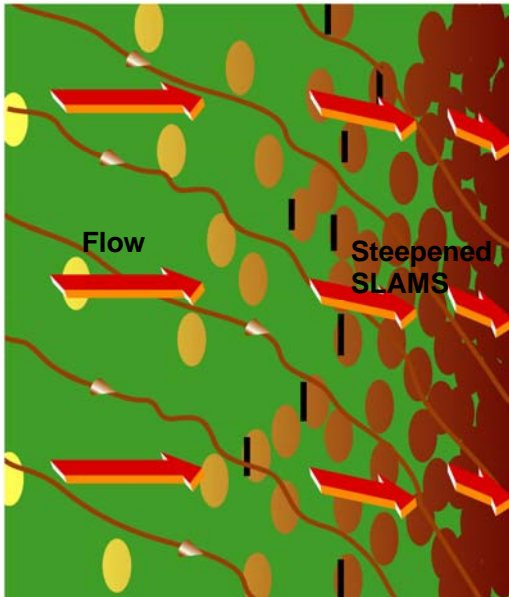

Figure 2. Schematic of the structure of a quasi-parallel shock [courtesy of S. J. Schwartz].

In this picture the shock is composed of an ensemble of SLAMS which grow and steepen through interaction with the energetic particle pressure gradient [14] as they are convected anti-sunwards. The patchwork of SLAMS act to decelerate and deflect the flow, and the shock transition is intrinsically extended in space and reforming in time. The larger SLAMS start to stand in the flow, and eventually become embedded in thermalised, downstream-like plasma. An initial suggestion for SLAMS overall extent, based on observations of the ULF waves from which they grow, was approximately 0.5 x 1 R_E [13]. However, it was found that they typically have a shorter correlation

length, of ~1000 km, than the ULF waves [15]. More recent simulations [12] suggest that their size is closer to 1000x3000 km, and that they become refracted as they approach the nominal bow shock location.

At the time of the Cluster launch many properties of SLAMS had not been measured directly. For example, their overall size, their shape, and whether they were uniform structures, as suggested by their monolithic profile. Simulations results predicted that they would have a rapid growth rate of the order of a few seconds [16], but this had not been measured directly, and the evolution of their properties with time was unknown. Most importantly, their effect on the plasma, and the process by which plasma was thermalised, was not well understood. Cluster has not yet allowed us to answer all of these questions, but in this paper we summarise some of the findings so far.
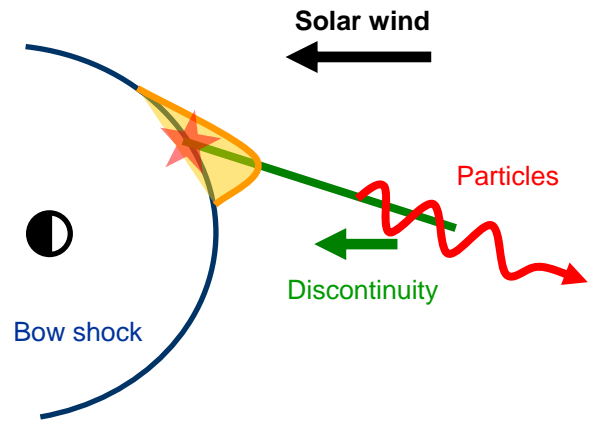

Figure 3. Schematic of the formation of an HFA.

The second bow shock phenomena to be discussed are Hot Flow Anomalies. The schematic in Figure 3 demonstrates the generation mechanism. HFAs are transient perturbations of the bowshock caused by its interaction with a tangential discontinuity (TD) embedded within the inflowing solar wind plasma. They were first identified using data from the ISEE and AMPTE missions [4,5] and an explanation for their generation mechanism was developed as a result of both observations and modelling work [17,18,19,20]. HFA formation is described in detail in [20], and only summarised briefly here.

HFAs are formed when the normal to the plane of an interplanetary tangential discontinuity (TD) is inclined at a large angle to the solar wind flow vector. As a consequence the line along which the discontinuity intersects with the shock tracks slowly across the bow shock. If, in addition, the discontinuity is thin relative to the gyroradius of an ion reflected from the bow shock, and the magnetic field orientation on either or both sides of the TD is such that the motional electric field experienced by reflected ions is directed towards the plane of the TD, then these ions can be focussed

towards the discontinuity plane. If the tracking velocity of the discontinuity is slow relative to the velocity of reflected ions, then a significant number of ions can stream away from the shock along the discontinuity. This additional ion population mixes with the incoming solar wind beam, and the overpressure drives an explosively expanding cavity filled with hot plasma.

Observationally HFAs are characterised by a hot, low density cavity, bounded by compressions in magnetic field and plasma density, with evidence for a magnetic field discontinuity embedded within the event. The compression on the exit edge (propagating against the solar wind in the plasma frame) is often larger than that on the entry edge, and develops into a shock if the expansion rate is great enough. HFAs frequently exhibit velocities deflected well away from the solar wind flow vector.

Multi-point Cluster data at a tetrahedron scale of 100 km were used to measure the shape and size of two events observed on one orbit [21]. Also presented are some unpublished data taken when the spacecraft were 5000 km apart, which show the development of an HFA as it passed over the tetrahedron. In the following two sections first SLAMS are discussed, followed by HFAs. This paper consists mainly of review material, supplemented by a few new results as yet unpublished.

2. PROPERTIES OF SLAMS

2.1 Observations of SLAMS at different tetrahedron scales

Figure 4 shows examples of the magnetic field strength of SLAMS observed at different tetrahedron scales. When the satellites were only 600 km apart (top panel), although each SLAM structure was observed by all four spacecraft, unexpectedly there were significant differences between the four observations. This immediately suggested that although the overall SLAMS size exceeded 600 km, there was significant internal structure [22]. The differences also made it difficult to measure the orientation of the SLAMS – relevant to understanding the ordering and evolution of the SLAMS as they approach the shock.

When the spacecraft were only 100 km apart (bottom panel) then the traces were far more similar, thus making it possible to measure the SLAMS orientation. In this case, however, the time differences were very small, leading to large uncertainties in the timing normal. In addition, the substantial scatter of orientations suggests that at this small scale, Cluster was sensitive to the local orientation of each SLAM structure, but analysis of these results is still ongoing. The small differences between SLAMS observed when the tetrahedron scale was only 100 km did allow a

measurement to be made of the scale on which gradients in the magnetic field strength occurred, as described by Lucek et al. [23]. These results will be described in the section 2.2.
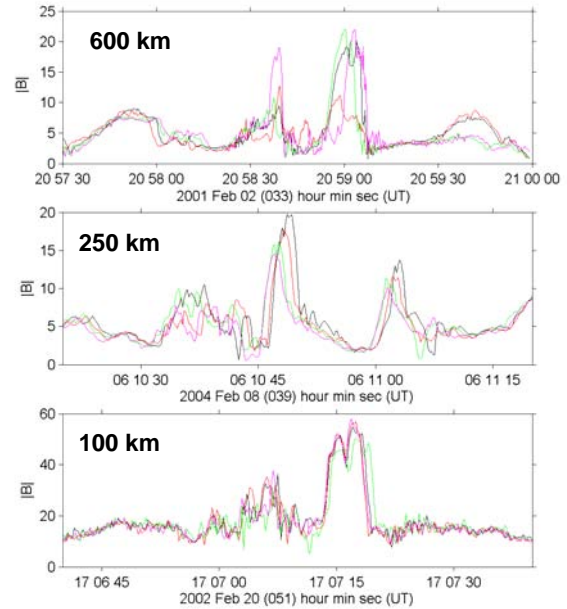
Figure 4. The magnetic field magnitudes of SLAMS observed at different tetrahedron scales. The four colours represent data from the four Cluster spacecraft.

Belhke et al. [24] made a comparison between the magnetic field magnitude trace and measurements of the spacecraft potential from EFW [25], the latter being a proxy for plasma density. They also studied the electric field measurements made by EFW, revealing further SLAMS structure. Figure 5 shows the magnetic field magnitude and spacecraft potential profiles for two of the intervals in Figure 4. The plasma density increase was in phase with |B|, consistent with the SLAMS being a fast mode structure, as expected. The plasma density also showed significant differences between the spacecraft at 600 km separation, but relative differences between |B| and $-V_{sp}$ were not correlated, suggesting that the different plasma parameters had different substructure [24]. This is most clearly seen in the top panel where the magnitude of the SLAMS in |B| is smaller at Cluster 1 than at Cluster 3 or 4, whilst the magnitude of $-V_{sp}$ is approximately the same at these three spacecraft.

Timing analysis was used to derive the velocity of the SLAMS in the top panel of Figure 5. As expected, this differed from the solar wind velocity, and the SLAM structure was found to be propagating sunward in the plasma frame. The motional electric field computed using the SLAMS velocity matched the measured electric field within the SLAMS, while a systematic

4

discrepancy was found if the motional electric field was calculated using the background solar wind velocity. Behlke et al [24] inferred therefore that, locally, the plasma within the SLAMS moved at the same speed as the SLAMS perturbation, although the SLAMS moved relative to the solar wind. The authors also noted that in some cases there was a depletion in the plasma density behind the SLAMS (in the SLAMS frame) indicating some kind of wake structure, and the presence of differences between the four spacecraft suggested that this wake varied on scales of ~600 km.
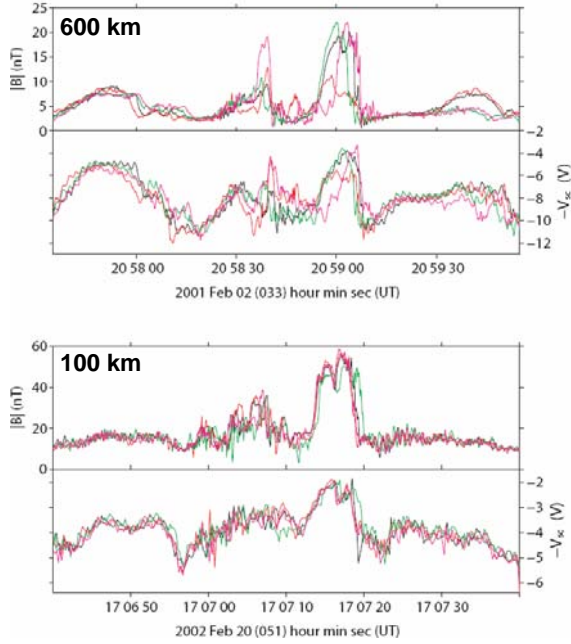

Figure 5. SLAMS observed at two different tetrahedron scales. The top panel of each pair shows magnetic field magnitude |B|, and the bottom panel the negative spacecraft potential, -V_{sp}, a proxy for plasma density.

Finally, comparison of the magnetic field signatures of the SLAMS when the spacecraft were 250 km apart, often showed evidence for growth of the SLAMS over the time scale of a few seconds (e.g. Figure 4, middle panel). Although not every case exhibited growth, the signature was sufficiently strong to allow an estimate of the growth rate to be made. These results will also be presented briefly in section 2.3.

2.2 Gradient scale in SLAMS

The examples shown in the previous section demonstrate that SLAMS have substantial internal structure, visible in both magnetic field and density data on scales of 600 km and less. One property of SLAMS which has been estimated is the typical scale on which gradients in the magnetic field occurred. Following the same analysis as described in [23], the probability distribution of differences in SLAMS size between two spacecraft was estimated. In order to expand the

statistics, the analysis was applied to an expanded sample of SLAMS measured when the tetrahedron scale was 100 or 250 km. The results presented in [23] only used SLAMS measured during one shock encounter on February 3 2002, when the spacecraft were separated by about 100 km. The results presented here incorporate SLAMS measured during several shock encounters in 2004 when the spacecraft separation was 250 km. The results show the same trend as the earlier study, but extend to larger scales.
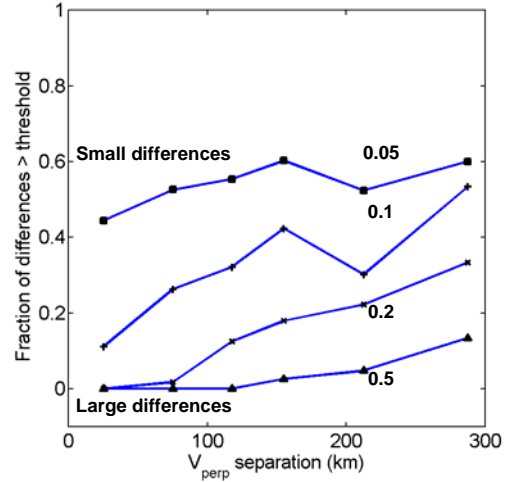

Figure 6. The change in occurrence of differences between spacecraft as a function of spacecraft separation perpendicular to the flow. Each trace shows the fraction of observed differences between pairs of spacecraft which exceed a certain threshold: 0.05, 0.1, 0.2, and 0.5, each plotted as a function of flow perpendicular separation.

Figure 6 was derived using the following method. For each SLAM structure the size of the signature observed by each of the four spacecraft was estimated. Then the SLAMS duration was calculated. This was done by finding the time for which the magnetic field magnitude exceeded half the maximum |B| observed by any of the spacecraft within the event. This gave an underestimate of the duration but avoided including effects of high frequency whistler waves which can occur at either the leading or trailing edges of the SLAMS. The integrated magnetic flux was then estimated for each event. The differences in flux between the different pairs of spacecraft were normalised by the maximum observed. Finally the probability of the normalised difference exceeding certain thresholds: 5%, 10, 20 and 50% was calculated as a function of spacecraft separation in a direction perpendicular to the solar wind flow.

Figure 6 shows the proportion of inter-spacecraft differences exceeding each threshold, plotted as a function of the spacecraft separation transverse to the solar wind flow. Small differences of only 5 or 10% occurred frequently, and did not show a strong

dependence on the separation of the spacecraft perpendicular to the flow. Large differences of 20 or 50%, however, were rarely seen unless the spacecraft were separated by 100-150 km perpendicular to the flow, and occurred more frequently at large separations. It was concluded therefore that gradients in |B| occurred on scales of 100-150 km, which was of the order of the ion inertial length.

These data include the effects of evolution of the structures in the time between the SLAMS being observed at the two spacecraft. One might expect spacecraft separated by a significant distance parallel to the solar wind velocity to be most sensitive to time evolution or growth of the SLAMS. It would have been better to have been able to remove from the sample those points derived when the two spacecraft had a large separation parallel to the plasma flow, and thus to gain a better estimate of the gradient. However, it was found that the flow parallel and flow perpendicular separations were not independent in this relatively small data set, and that no conditioning of the data by flow parallel separation was possible in this case.

2.3   SLAMS growth rate

Figure 4 shows that when the Cluster spacecraft were separated by 250 km some SLAMS showed evidence for growth as they passed over the four spacecraft. A variety of signatures were observed: the SLAMS profile often changed shape as it grew, and not all SLAMS showed clear evidence for growth on these timescales. Thus growth is perhaps unlikely to be at a constant rate. However, an initial attempt to identify a statistically significant signature of SLAMS growth was made using a sample of SLAMS from 5 quasi-parallel shocks, observed during 2004.

For each observation of a SLAM structure by a pair of spacecraft, the ratio between the SLAMS magnitudes at the two spacecraft was calculated and plotted as a function of the time between the observations. Ratios exceeding one therefore indicate a signature consistent with growth. The data are plotted in Figure 7.

Figure 7 shows a trend consistent with the growth of the SLAMS in the time between being observed by the two satellites. A least squares, straight line fit gives a gradient of $0.27\pm0.04s^{-1}$. This is a statistically significant slope suggesting that locally SLAMS grow on timescales of a few seconds, consistent with results from simulations [16]. The slope is not sensitive to the separation of the spacecraft perpendicular to the flow. We attribute this to the correlation between flow parallel and flow perpendicular separations, and the rather patchy sampling of this parameter space. We would expect SLAMS growth and spatial variations to affect the results shown in Figures 6 and 7 respectively, but with our current sample of SLAMS we are not able to

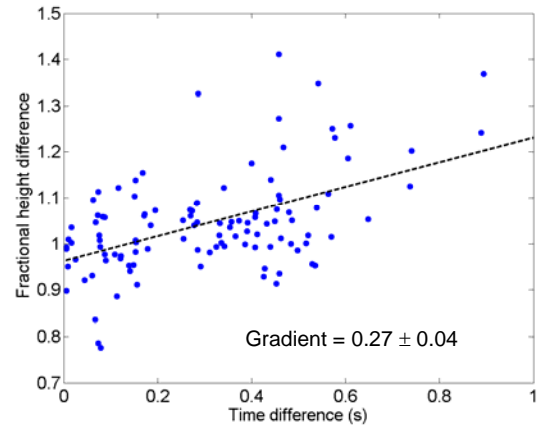examine the spatial structure and growth of SLAMS independently.

Figure 7. Fractional differences in the sizes of SLAMS between pairs of spacecraft, measured by the SLAMS peak magnetic field magnitude, plotted as a function of time difference between the observations.

3.   PROPERTIES OF HFAS

As found for the analysis of SLAMS, measurements of HFAs made using different tetrahedron scales are suited to examining different aspects of HFA formation and evolution. When the spacecraft were relatively close together, at 600 km or smaller for example, then the HFA signatures at the different spacecraft were often similar enough to be able to calculate the orientation and speed of the compressions at the edge of the HFA [21]. In contrast, when the spacecraft were far apart, separated by 5000 km for example, then an HFA developed significantly in the time taken for it to cross the Cluster tetrahedron, allowing its time evolution to be studied. We give an example of each kind of analysis. Statistical analysis of a sample of events is ongoing.

3.1   HFA structure and motion

The first set of HFAs to be presented here were observed on April 2 2002 at a time when the Cluster tetrahedron scale was ~100 km. Cluster had just exited the bow shock at high northern latitudes: (+9.9, -2.2, +8.11) R_E in GSE. Several HFAs were observed of varying complexity.

Example 1

Figure 8 shows magnetic field and plasma data for the first HFA, observed closest to the bow shock. Cluster entered the HFA through a weak compression at ~03:36:15 UT and exited through a shock, at ~03:36:50 UT. Between these transitions Cluster observed a region of hot plasma, but low magnetic field and ion number density.

Examination of the ion distributions from the CIS HIA sensor showed that before entering the cavity Cluster observed a single population of ions, corresponding to the anti-sunward propagating solar wind beam (Figure 9a).
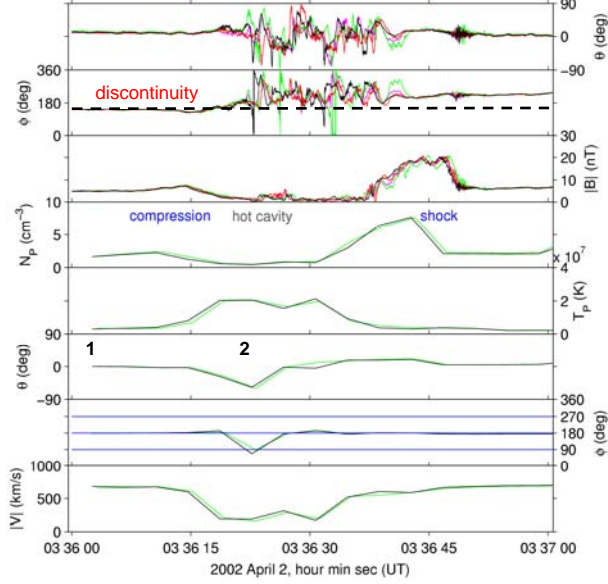

Figure 8. An example of an HFA. Panels show magnetic field elevation and longitude angles in degrees (θ, φ), magnetic field magnitude (|B|), ion number density (Np), ion temperature (Tp), velocity elevation and longitude angles (θ, φ), and velocity magnitude |V| in km/s. The horizontal dashed line in panel 2 highlights the change in magnetic field direction across the event. The numerals 1 and 2 indicate the approximate times of the ion distributions shown in Figure 9.

The apparent velocity flow deflection seen within the cavity can be explained by the presence of two ion populations: the solar wind beam, and a beam of sunward flowing ions, consistent with ions reflected from the shock being focused along the discontinuity (Figure 9b). The densities of the two populations were approximately equal. Such an ion distribution is unstable to wave generation which would tend to scatter the ions, forming a single distribution: the cavity already showed some evidence of wave activity, and HFAs later on the same orbit contained a single, hot plasma population. Since the two ion populations were distinct in this case it was suggested that this HFA was relatively young [21].

It was assumed that the discontinuity underlying this HFA was a tangential discontinuity (TD), as expected from simulations of HFA generation [18]. Based on this assumption the normal to the discontinuity was calculated from the cross product of the magnetic field direction upstream and downstream of the HFA. The

orientation of the TD was then used to calculate the velocity of the line of interaction between the discontinuity and the bow shock. The motional electric field experienced by ion reflected from the bow shock was calculated from the magnetic field observed on either side of the HFA and the measured solar wind velocity. In addition, timing analysis was used to calculate the orientation and speed of the edges, for comparison with the observed plasma motion within the HFA core.
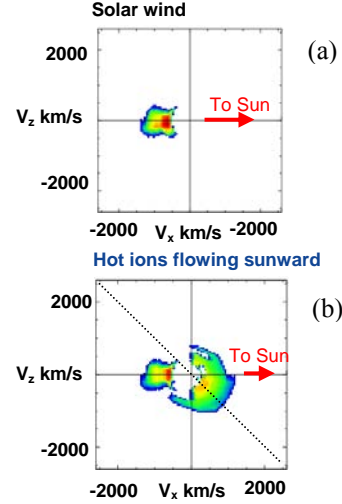

Figure 9. Two cuts through Cluster 3 CIS HIA ion distributions in the X-ZGSE plane (YGSE = 0), measured (a) outside the HFA cavity, showing the solar wind beam propagating anti-sunward; and (b) inside the cavity, showing a weakened ion beam and an additional population of ions propagating sunward.

The derived properties of this HFA are briefly summarised in the following paragraphs and summarised in the sketch in Figure 10. The discontinuity normal was found to lie mainly in the GSE-Z direction, largely confined to the XZ-plane, $n_{dis1}=(0.17,−0.07,0.98)_{GSE}$. Since Cluster was near noon the sketch of this HFA could be projected onto the XZ-plane. The discontinuity first intersected the bow shock along a line northwards of Cluster, then tracked southwards at a speed of ~110 km s^{-1}.

Assuming that the HFA did not develop significantly during the time it took to cross the spacecraft, which was supported by the similar magnetic profile seen at all four spacecraft, the Cluster data were projected onto a vertical cut through the HFA structure. It was then possible to transform from the time profile in Figure 8 to the spatial schematic shown in Figure 10. Projected onto the spacecraft track are the perturbations to the velocity vectors: these are the instantaneous differences between the local velocity vector and the solar wind velocity outside of the HFA. The filled grey circle indicates the satellite location at the time the HFA was observed. Also shown in Figure 10 is a cut through a

model bow shock surface, estimated for the time at which Cluster crossed into the solar wind just a few minutes earlier. The satellite therefore appeared to be close to the bow shock at this time, as was also expected from the observation of two ion populations within the cavity.
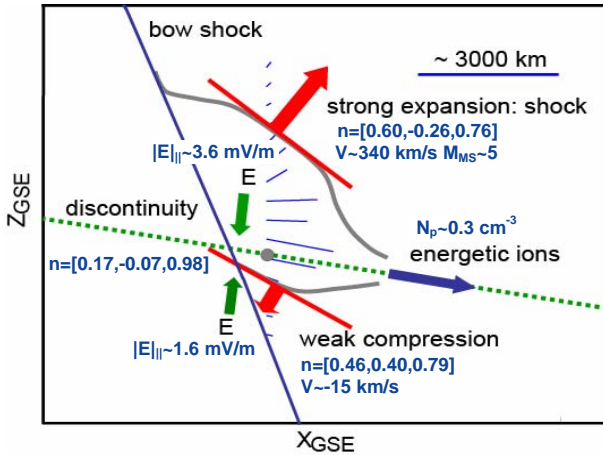

Figure 10. HFA properties derived from Cluster observations.

The orientations of the edges of the HFA cavity were calculated using four spacecraft timing analysis, together with the speed of motion along their normals. These orientations in the XZ-plane are indicated on Figure 10 at the time along the satellite track when they were observed. Cluster encountered a weak compression at the start of the HFA, which had a normal n_a=(0.46,0.40,0.79), travelling at only -15 km s^{-1} in the solar wind frame, i.e. anti-sunward. Cluster exited through a shock, with a normal n_b = (0.60,−0.26,0.76), travelling sunward at 340 kms^{-1} in the solar wind frame, corresponding to a magnetosonic Mach number of ~5.

The vertical scale of the HFA (~3000 km) was calculated from its duration and from the estimated speed at which the discontinuity was expected to track across the tetrahedron. However, the orientations of the magnetic compression at the start of the HFA and the shock at the end were found to be close to parallel to the estimated orientation of the underlying discontinuity, consistent with them being generated by expansion of the cavity perpendicular to the discontinuity plane. In addition, the perturbations to the plasma velocity projected onto the track of the tetrahedron through the cavity show flow along the discontinuity plane near the centre of the cavity, and flow consistent with strong expansion nearer the edges. We therefore suggest that the extent of the HFA in the Y and X directions is larger than its scale in Z. Comparison of the Y components of the normals found for the edges, however, shows a change in sign, which might be a signature of non-planarity of the HFA cavity.

Example 2

The second HFA, also observed on April 2 2002, when the spacecraft had a separation of the order of 100 km, was rather more complex than the example presented in the previous section. Figure 11 shows the magnetic field data for this event, in the same format as Figure 8 except that in this case the shaded region indicates the HFA. A second HFA-like event occurred later in the interval, but that event is not discussed here. The same analysis was applied to the data from this HFA as described in the previous section. The normal to the underlying discontinuity was calculated from the cross product of the upstream and downstream magnetic field vectors. The magnetic field was steady before the first HFA was observed, but the spacecraft only made a brief entry into the solar wind between the two HFAs in this interval. The value for the downstream field was calculated from the average field during approximately 30 seconds after the end of the shaded region, despite the presence of ULF waves characteristic of the ion foreshock.
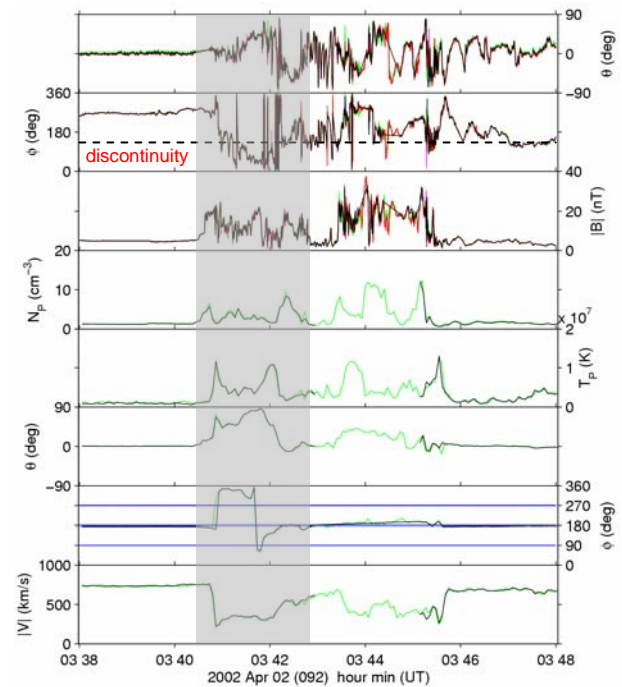

Figure 11. Cluster magnetic field and plasma data for an HFA in the same format as Figure 8. The horizontal dashed line highlights the presence of a discontinuity within the HFA, indicated by the shaded region.

The discontinuity normal was found to be n_{dis2}=[0.02,0.02,1.00]$_{GSE}$: almost entirely in the Z_{GSE} direction. Consequently the estimate for the velocity at which the discontinuity tracked across the bow shock was very slow, with a large error. However, calculation of the orientation and speed of the two part compression through which Cluster entered the HFA showed that the entry edge crossed northwards across the Cluster

tetrahedron, implying that the discontinuity first intersected the bow shock at a location to the south of Cluster, and then tracked northwards across the bow shock. The discontinuity normals and speeds for the two part entry compression were: n_1=[0.01, 0.01, 1.00]; $V.n_1$ ~ 145 km/s and n_2=[0.04, 0.11, 0.99]; $V.n_2$ ~ 305 km/s. The high velocity of the second compression identified it as a shock, with a magnetosonic Mach number M_{MS}~5. The first, weaker compression might therefore represent a shock foot structure.
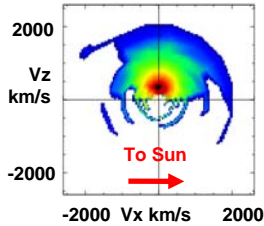

Figure 12. A cut through Cluster 3 CIS ion distributions, in the X-Z_{GSE} plane (Y_{GSE} = 0), showing a single hot ion distribution inside the HFA cavity. The velocity moment of this distribution has a northward component.

Examination of the CIS HIA ion distribution inside the cavity, shown in Figure 12, indicated that at this time there was only a single, hot ion distribution present, which had a northwards velocity component. The velocity perturbation shown in Figure 11 indicates a strong flow deflection northward, and then a small deflection southward. These results are consistent with the HFA having an overall northward velocity, yet simultaneously expanding rapidly northwards and southwards perpendicular to the discontinuity plane.

3.2   HFA time evolution

Finally we briefly present an example of an HFA observed when the Cluster tetrahedron scale was 5000 km, and the HFA was seen to evolve over a timescale of the order of a minute or so. Figure 12 has four panels, each of which shows the magnetic field magnitude observed by each of the four Cluster spacecraft. The order in which the satellites observed the HFA was 4-3-2-1. This time order was consistent with the tetrahedron configuration and location at the time and the estimated orientation of the discontinuity which was embedded within the HFA. When the HFA was observed by the first satellite (Cluster 4) it was bounded by two modest compressions. However, in the time it took the HFA to pass over the three remaining spacecraft it also evolved. The exit compression developed into a shock-like transition, although with data from only a single spacecraft it is difficult to unambiguously identify the exit transition as a shock, and the appearance of the cavity and waves within the cavity evolved significantly. Measurement of the evolution rates of HFAs using data at large separations is ongoing.
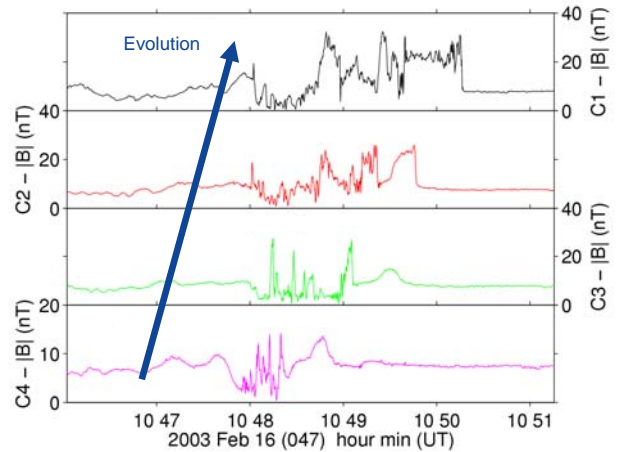

Figure 13. Example of the evolution of an HFA as it crossed the Cluster tetrahedron. Panels 1 to 4 show the magnetic field magnitude (in nT) from Cluster 1 (black), 2 (red), 3 (green) and 4 (magenta), respectively. The time order of the observations is Cluster 4, 3, 2 and finally Cluster 1.

4.   SUMMARY AND CONCLUSIONS

4.1   The quasi-parallel shock and properties of SLAMS

One of the processes which govern plasma thermalisation at the quasi-parallel shock is the self-generation of magnetic pulsations or SLAMS by the shock, through the interaction of upstream waves with a gradient in energetic particle pressure. In this paper results regarding the properties of these pulsations have been presented. It was found that data recorded at different spacecraft separation scales were sensitive to different properties of the SLAMS and consequently observations at different tetrahedron scales are suited to studying different aspects of SLAMS structure.

SLAMS are fast mode structures, with correlated magnetic field magnitude and density enhancements and overall extents exceeding 1000 km, but they showed significant internal structure on scales of 600 km and smaller, with significant differences between the magnetic field and density profiles on these scales. Thus they exhibit variations on smaller scales than the foreshock ULF waves from which they are thought to grow [22,24].

When the Cluster spacecraft were close together, of the order of 100 km, the magnetic field signatures were generally very similar. In principle this allowed a measurement of the orientation and motion of the structures to be made. However, it was found that the small time differences between the SLAMS being observed at different spacecraft led to large errors in the normal determination. Also, it appeared that at these small scales, the orientation analysis was most likely to

be sensitive to local ripples in the SLAMS structure, and no large scale ordering of SLAMS orientation was found. Therefore it was not possible to establish whether refraction of the SLAMS occurred as they were convected towards the shock, as predicted by simulation results [12]. Data from small spacecraft scales could be used, however, to give an indication of the scale on which significant gradients occurred within the SLAMS. Analysis of data recorded at 100 and 250 km scales both indicated that gradients occurred on the order of 100-150 km, approximately the scale of a thermal ion gyroradius [23].

SLAMS observed at parallel shocks under conditions when the spacecraft were of the order of 250 km apart showed signatures consistent with growth of the structures as they crossed the tetrahedron. Analysis of the fractional change in amplitude between pairs of spacecraft, plotted as a function of the time difference between the observations showed that, despite it being likely that SLAMS grow sporadically rather than at a constant rate, a significant signature of growth was determined. The gradient of a fit to the scatter plot was used to infer a growth rate exceeding a factor of 0.25 per second.

The properties of SLAMS are only one aspect to understanding the themalisation processes operating at the quasi-parallel shock. SLAMS are known to be associated with reflected ions, but the importance of these ions to the shock is not yet known. Recent work by Behlke et al. [26] also showed that SLAMS were associated with ion solitary waves (SWs) moving parallel to **B** at speeds exceeding the typical ion thermal speed. These SWs cannot be explained by any of the current SW models, and whether they play a significant rôle in plasma thermalisation has yet to be determined. Understanding the details of how the time varying 'patchwork' of SLAMS mediates the deceleration and deflection of the solar wind plasma still remains an open question.

4.2   Properties of HFAs

Although HFAs have been studied using in-situ observations and simulations for over a decade, Cluster measurements allow us to characterise HFA properties not previously possible. Using the four-point data to measure the orientation and motion of the edges of the cavity allowed HFA expansion rates, topology, and scale to be studied. In addition, multiple single spacecraft observations of the same event allowed HFA time evolution to be explored. Statistical analysis is in progress and here several examples of the type of analysis possible with Cluster have been presented.

Measurements of two HFAs when the spacecraft were approximately 100 km apart were used to infer the orientation of the edges of the cavity for comparison

with the estimated orientation of the underlying discontinuity embedded within the HFA. Results suggested that locally the HFA had the form of an expanding sheet centred on the discontinuity, with a thickness perpendicular to the discontinuity of approximately 3000 km. The speed of the edges, together with measurement of the bulk velocity perturbation is consistent with HFA motion being a superposition of convection across the bow shock and expansion perpendicular to the discontinuity plane. Expansion can be sufficiently rapid to drive a shock at the edges [21].

Considering the ion distributions inside the cavity, one HFA had two ion distributions of approximately equal density within its core: a solar wind beam, and a population of ions flowing sunward which were interpreted as ions that had been reflected from the bow shock and then focussed along the discontinuity. Another HFA contained a single, hot population, with a velocity moment consistent with the inferred tracking velocity of the HFA across the bow shock. This second example appeared to be more developed, and it was suggested that an HFA with two ion populations in the cavity was an event at an early stage of development, consistent with the location of Cluster very close to the bow shock [21]. The two ion distributions would be expected to mix, forming a single, hot distribution, as observed in the second example.

Finally, when the spacecraft were 5000 km apart, an example of an HFA was presented which had signatures consistent with its evolution in the time taken to cross the tetrahedron. Over the order of a minute the wave power inside the HFA changed, the ion distributions evolved and the weak compression at the exit edge grew into a strong compression which had the appearance of a shock. In this case though, it was not possible to definitely demonstrate the evolution of a dual ion population into a single ion population.

In conclusion, some of the contributions made by Cluster to the understanding of SLAMS and HFAs have been described. However, there is still much to be done including statistical analysis and examination of these structures at other tetrahedron scales. In particular though, the next step is to understand the results on the properties of these structures in the broader context of shock physics.

6. REFERENCES

1. Schwartz, S. J., and Burgess, D., Quasi-parallel shocks: A patchwork of three-dimensional structures, *Geophys. Res. Lett.*, Vol. 18, 373–376, 1991.

2. Thomsen, M. F., Gosling, J. T., and Russell, C. T., ISEE studies of the quasi-parallel bow shock, *Adv. Space Res.*, Vol. 8, 9175–9178, 1988.

3. Schwartz, S. J., et al., An active current sheet in the solar wind, *Nature*, Vol. 318, 269–271, 1985.

4. Thomsen, M. F., Gosling, J. T., Fuselier, S. A., Bame, S. J., and Russell, C. T., Hot, diamagnetic cavities upstream from the Earth's bow shock, *J. Geophys. Res.*, Vol. 91, 2961–2973, 1986.

5. Paschmann, G., Haerendel, G., Sckopke, N., Möbius, E., Lühr, H., and Carlson, C. W., Three-dimensional plasma structures with anomalous flow directions near the Earth's bow shock, *J. Geophys. Res.*, Vol. 93, 11,279–11,294, 1988.

6. Paschmann, G., Sckopke, N., Bame, S. J., and Gosling, J. T., Observations of gyrating ions in the foot of the nearly-perpendicular bow shock. *Geophys. Res. Lett.*, Vol. 9, 881-884, 1982.

7. Le, G., and Russell, C. T., A study of the coherence length of ULF waves in the Earth's foreshock, *J. Geophys. Res.*, Vol. 95, 10703–10706, 1990.

8. Greenstadt, E. W., Hoppe, M. M., and Russell, C. T., Large-amplitude magnetic variations in quasi-parallel shocks: correlation lengths measured by ISEE 1 and 2, *Geophys. Res. Lett.*, Vol. 9, 781–784, 1982.

9. Balogh, A., et al., The Cluster Magnetic Field Investigation: Overview of in-flight performance and initial results, *Ann. Geophys.*, Vol. 19, 1207–1217, 2001.

10. Rème, H., et al., First multispacecraft ion measurements in and near the Earth's magnetosphere with the identical Cluster ion spectrometry (CIS) experiment, *Ann. Geophys.*, Vol. 19, 1303– 1354, 2001.

11. Giacalone, J., Schwartz, S. J., and Burgess, D., Observations of suprathermal ions in association with SLAMS, *Geophys. Res. Lett.*, Vol. 20, 149–152, 2001.

12. Dubouloz, N., and M. Scholer, M., Two-dimensional simulations of magnetic pulsations upstream of the Earth's bow shock, *J. Geophys. Res.*, Vol. 100, 9461–9474, 1995.

13. Schwartz, S. J., and Burgess, D., Quasi-parallel shocks: A patchwork of three-dimensional structures, *Geophys. Res. Lett.*, Vol. 18, 373–376, 1991.

14. Burgess, D., Cyclic behaviour at quasi-parallel collisionless shocks, *Geophys. Res. Lett.* Vol. 16, 345–348, 1989.

15. Greenstadt, E. W., Hoppe, M. M., and Russell, C. T., Large-amplitude magnetic variations in quasi-parallel shocks: correlation lengths measured by ISEE 1 and 2, *Geophys. Res. Lett.*, Vol. 9, 781–784, 1982.

16. Giacalone, J., Schwartz, S. J., and Burgess, D., Artificial spacecraft in hybrid simulations of the quasi-parallel Earth's bow shock: Analysis of time series versus spatial profiles and a separation strategy for Cluster, *Ann. Geophys.*, Vol. 12, 591–601, 1994.

17. Burgess, D., On the effect of a tangential discontinuity on ions specularly reflected at an oblique shock, *J. Geophys. Res*, Vol. 94, 472–478, 1989.

18. Thomas, V. A., Winske, D., Thomsen, M. F., and Onsager, T. G., Hybrid simulation on the formation of a hot flow anomaly, *J. Geophys. Res.*, Vol. 96, 11,625–11,632, 1991.

19. Thomsen, M. F., Thomas, V. A., Winske, D., Gosling, J. T., Farris, M. H., Russell, C. T., Observational test of hot flow anomaly formation by the interaction of a magnetic discontinuity with the bow shock, *J. Geophys. Res.*, Vol. 98, 15,319–15,330, 1993.

20. Schwartz, S. J., Paschmann, G., Sckopke, N., Bauer, T. M., Dunlop, M., Fazakerley, A. N., and Thomsen, M. F., Conditions for the formation of hot flow anomalies at Earth's bow shock, *J. Geophys. Res.*, Vol. 105, 12,639–12,650, 2000.

21. Lucek, E. A., Horbury, T. S., Balogh, A., Dandouras, I., and Rème, H., Cluster observations of hot flow anomalies, *J. Geophys. Res.*, pp. A06207, doi:10.1029/2003JA010016, 2004.

22. Lucek, E. A., Horbury, T. S., Dunlop, M. W., Cargill, P. J., Schwartz, S. J., Balogh, A., Brown, P., Carr, C., Fornacon, K. -H., and Georgescu, E., Cluster magnetic field observations at a quasi-parallel bow shock, *Ann. Geophys.*, Vol. 20, 1699–1710, 2002.

23. Lucek, E. A., Horbury, T. S., Balogh, A., Dandouras, I., and Rème, H., Cluster observations of structure at quasi-parallel bow shocks, *Ann. Geophys.*, Vol. 22, 1-5, 2004.

24. Behlke, R., André, M., Buchert, S. C., Vaivads, A., Eriksson, A. I., Lucek, E. A., and Balogh, A., Multi-point electric field measurements of Short Large-Amplitude Magnetic Structures (SLAMS) at the Earth's quasi-parallel bow shock, *Geophys. Res. Lett.*, Vol. 30, 1177, doi:10.1029/2002GL015871, 2003.

25. Gustafsson, G., et al., The Electric Field and Wave experiment for the Cluster mission, *Space Sci, Rev.*, Vol. 79, 137–156, 1997.

26. Behlke, R., André, M., Bale, S. D., Pickett, J. S., Cattell, C. A., Lucek, E. A., and Balogh, A., Solitary structures associated with short large-amplitude magnetic structures (SLAMS) upstream of the Earth's quasi-parallel bow shock, *Geophys. Res. Lett.*, Vol. 31, L16805, doi:10.1029/2004GL019524, 2004.